A Fast Load-Pull Optimization for Power-Added Efficiency Under Output Power and ACPR Constraints

MATTHEW FELLOWS, Student Member, IEEE
LUCILIA LAMERS, Student Member, IEEE
CHARLES BAYLIS, Member, IEEE
LAWRENCE COHEN, Senior Member, IEEE
ROBERT J. MARKS II, Fellow, IEEE
Baylor University
Waco, TX USA

In the future real-time optimization of reconfigurable radar transmitter power amplifiers, a typical optimization would seek the highest power-added efficiency (PAE) possible under constraints on adjacent-channel power ratio and delivered power. This paper describes a sequential, fast optimization algorithm to find the constrained optimum using experimental queries taken at sequentially selected load reflection-coefficient values. The algorithm is compared across multiple starting reflection-coefficient values on the Smith chart and convergence to similar constrained optimum impedances and PAE values is demonstrated in both simulation and measurement. This algorithm is designed to allow reconfigurable radar transmitter amplifiers to optimize in real-time, meeting dynamically changing spectral mask, power efficiency, and output power requirements.

Manuscript received May 4, 2015; revised November 4, 2015, February 19, 2016; released for publication August 7, 2016.

DOI. No. 10.1109/TAES.2016.150313.

Refereeing of this contribution was handled by A. Charlish.

This work has been funded under a grant from the National Science Foundation (Award Number ECCS-1343316). The authors would like to thank Keysight Technologies for the cost-free loan of the Advanced Design System simulation software.

Authors' address: Baylor University, Electrical and Computer Engineering, One Bear Place #97356, Waco, Texas 76798-7356 USA. Corresponding Author is C. Baylis at E-mail: (Charles_Baylis@Baylor.edu)

I. INTRODUCTION

In future cognitive and adaptive radar transmitters, the power amplifier will need to quickly reconfigure, maximizing performance in different frequency bands and under dynamically varying spectral and output power constraints. While adaptive radar has been an area of interest to the radar community since the 1970s [1], the microwave circuit technology to implement an adaptive radar is now maturing to the point where a fully adaptive radar is feasible. The reconfigurable amplifier must satisfy performance criteria in several key areas. Linearity allows spectrally confined transmission, power efficiency allows expeditious use of available energy, and output power is critical for target detection. Because these criteria are all significantly dependent on the load impedance seen by the device, real-time load impedance optimization can facilitate changing demands in these performance areas. The need to optimize the nonlinear circuitry of the power amplifier is part of a progression shown in the recent literature toward a joint circuit and waveform optimization for adaptive radar. Blunt et al. [2] have focused heavily on using the power-efficient and spectrally well-performing polyphase-coded frequency modulation (PCFM) waveforms and has demonstrated PCFM waveform optimization with the transmitter amplifier considered through modeling and also by using amplifier measurements [3].

To perform real-time optimization of impedance in a radar transmitter, a variable impedance matching circuit would be added between the power amplifier and the array combiner (or antenna if a single element is present in the array). Some scenarios for the technology to implement this matching circuitry have been demonstrated [4, 5], and implementation of the matching network in an adaptive radar platform is discussed thoroughly by Kingsley and Guerci [4]. From this work, it appears that tuning of typically useful matching circuits could be done on the order of microseconds. While the specific contribution of our present work is to discuss fast algorithms for tuning, these papers provide some examples of the platform in which these algorithms could be integrated.

A typical scenario might involve the maximization of power efficiency while meeting requirements on the adjacent-channel power ratio (ACPR) and delivered power. To accomplish this, a constrained optimization is presented that involves three input parameters. The optimization is executed by maximizing one input parameter while maintaining the other two input parameters within the imposed constraints. This solves a problem similar to Pareto optimization, which optimizes input parameters to find the best trade-off for multiple objectives [6–11]. In addition to the well-known variation of output power on the load impedance, both the power-added efficiency (PAE) and ACPR are also significantly dependent on load impedance [12]. PAE is

defined by the following equation:

$$PAE = \frac{P_{out,RF} - P_{in,RF}}{P_{DC}} \times 100\%. \quad (1)$$

PAE describes the efficiency of converting DC power to radio frequency power. The ACPR is the ratio of the power in the adjacent channel to the in-band power, and it is usually desirable to minimize this metric, which decreases with increasing amplifier linearity. Spectral spreading, which causes increased ACPR, results from nonlinearity-induced intermodulation between amplifier excitation frequency components in the main band. In addition to optimizing PAE and ACPR, the output power must be large enough to illuminate the target for an echo power discernable by the receiver.

We recently developed algorithms for the maximization of PAE under ACPR constraints [13, 14]: a two-criterion, constrained optimization. The present paper allows requirements on output power to also be specified and included in the optimization, creating a three-criterion, constrained optimization. PAE, ACPR, and input power are often considered simultaneously in power amplifier design. Sevic et al. [12] describe a traditional load-pull measurement, the variation of load impedance to minimize ACPR and maximize PAE under an output-power requirement. Iwamoto et al. [15] show a plot of PAE and ACPR versus output power for a Doherty amplifier under code-division multiple access (CDMA) excitation. Zhang et al. [16] and Noh and Park [17] describe linearization enhancement by using output power, PAE, and ACPR as metrics for performance. Kusunoki et al. [18] demonstrate the relationship between the power back-off level (in dB) and the ACPR as well as plotting both PAE and ACPR versus output power. All three of these criteria are considered in design; however, the input power is adjusted to provide the best combination, rather than the load impedance as the present paper discusses. The dependence of ACPR on load impedance [12, 19] and the relationship of ACPR two traditional two-tone assessments of third- and fifth-order intermodulation [20] have been shown. Reveyrand et al. [21] demonstrate the use of a fast load-pull optimization for obtaining maximum PAE under constraints on output power and dissipated power by generating regional models in the Smith chart using the large-signal S-parameters and strategic measurements at different load reflection coefficient values. The approach detailed in the present paper differs from the approach in [21] in the following ways: 1) no model is extracted in the present paper and 2) the present paper presents an approach that uses a spectral-spreading metric (ACPR) as one of its constraints.

Various fast, measurement-based impedance optimizations have also been demonstrated in the literature. Sun and Lau [22, 23] use a genetic algorithm to perform antenna matching based on voltage standing wave ratio measurements. Qiao et al. [24] present a reconfigurable amplifier and use a genetic algorithm for real-time reconfiguration. However, genetic algorithms have been observed to be slower than other candidate algorithms for some impedance-matching applications [25].

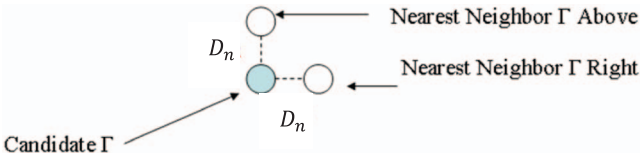

Fig. 1. Measured Γ_L points for PAE, ACPR, and P_d gradient estimation at candidate.

The remainder of the paper describes our optimization algorithm and presents results for its validation. Section II provides theoretical description of the optimization. Section III demonstrates simulation results for the algorithm. Section IV presents measurement results for the algorithm. Section V presents conclusions and suggestions for future work.

II. ALGORITHM DESCRIPTION

The algorithm is designed to search within the Smith chart for the load reflection coefficient Γ_L providing the largest value of PAE while remaining within constraints on the output power delivered to the load (P_d) and ACPR. The algorithm begins by requesting the following inputs: the neighboring-point resolution distance D_n, the step-size parameter D_s, the starting value for Γ_L, the maximum ACPR, and the minimum P_d. The algorithm proceeds based on estimation of the PAE, ACPR, and P_d gradients in the Smith chart. The estimation of these gradients requires measurements at two neighboring Γ_L points for each candidate, separated from the candidate by D_n in the $Re(\Gamma_L)$ and $Im(\Gamma_L)$ directions. Fig. 1 shows a conceptual sketch of these neighboring-point measurements used for the gradient estimations.

The search progresses from one candidate Γ_L to the next using the step-size parameter D_s, measurement results, and the estimated gradients. A search vector is added to the present candidate to find the subsequent candidate. This search vector depends on the acceptability of the P_d and ACPR values at the present candidate. If a candidate Γ_L provides values outside the specified limits for both ACPR and P_d, then the algorithm adds the search vector

$$\bar{v} - = \hat{a} D_a + \hat{d} D_d \quad (2)$$

to the candidate to obtain the next candidate, where $\hat{a}$ is the opposite of the ACPR gradient (direction of steepest descent for ACPR), $\hat{d}$ is the direction of steepest ascent for P_d, and

$$D_a = \frac{D_s}{2} \frac{|ACPR_{cand} - ACPR_{limit}|}{|ACPR_{worst} - ACPR_{limit}|} \quad (3)$$

$$D_d = \frac{D_s}{2} \frac{\left|P_{d,cand} - P_{d,limit}\right|}{\left|P_{d,worst} - P_{d,limit}\right|}. \quad (4)$$

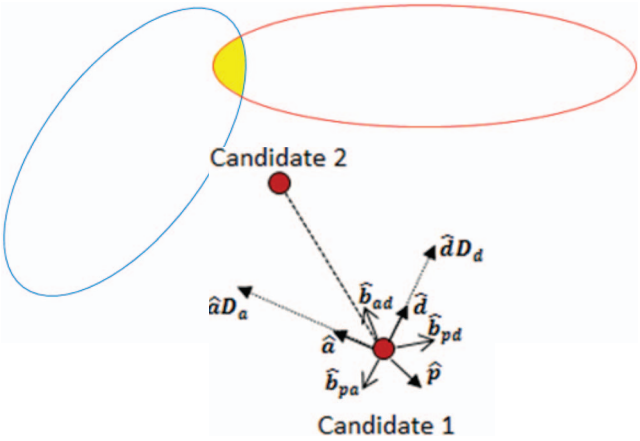

Fig. 2. Graphical representation of Smith chart step vectors used for determination, using (2), of new candidate point when originating candidate is outside both P_d and ACPR acceptable regions.

$ACPR_{cand}$ and $P_{d,cand}$ are the ACPR and delivered power values at the candidate, respectively. $ACPR_{limit}$ and $P_{d,\,limit}$ are the given constraints on ACPR and P_d. $ACPR_{worst}$ is the worst (highest) value of ACPR obtained over all measurements in the algorithm, and $P_{d,worst}$ is the worst (lowest) value of delivered power taken over all the measurements. As such, D_a and D_d estimate the fraction of the total distance that remains to the limit of ACPR or P_d based on the values at the measured candidate and the worst point measured multiplied by half of the step-size parameter D_s. The significance of the step-size parameter D_s is that it would be the length of the search vector if $\hat{a}$ and $\hat{d}$ were in the same direction in (2) and if $P_{d,cand}$ and $ACPR_{cand}$ (delivered power and ACPR at the candidate) take on the worst measured values recorded, as happens in the first candidate in each search. The vector $\bar{v}-$ defined in (2) pushes the search toward the mutually acceptable region for both ACPR and P_d. This scenario is illustrated in Fig. 2. In Fig. 2, $\hat{p}$ is the unit vector in the direction of the PAE gradient, and the $\hat{b}$ vectors are bisectors between the vectors indicated in their subscripts.

If the present candidate Γ_L possesses acceptable ACPR but unacceptable P_d, then the search vector becomes

$$\bar{v}- = \hat{d}D_d + \hat{b}_{ad}D_{b,ad}, \tag{5}$$

where D_d is specified by (4), $\hat{b}_{ad}$ is the vector bisecting $\hat{a}$ and $\hat{d}$, and

$$D_{b,ad} = \frac{D_s}{2}\frac{|\theta_{ad} - 90^\circ|}{90^\circ}, \tag{6}$$

where θ_{ad} is the angle between $\hat{a}$ and $\hat{d}$. The component $\hat{d}D_d$ forces the search to improve the value of P_d, and the component $\hat{b}_{ad}D_{b,ad}$ forces the search toward the Pareto front for ACPR and P_d. At the Pareto front between two objectives, the gradients for these objectives are collinear [13]. Thus, the bisector of the two gradients is expected to send the search toward the Pareto front linking the two optima. $D_{b,ad}$ is an estimator of the fractional distance

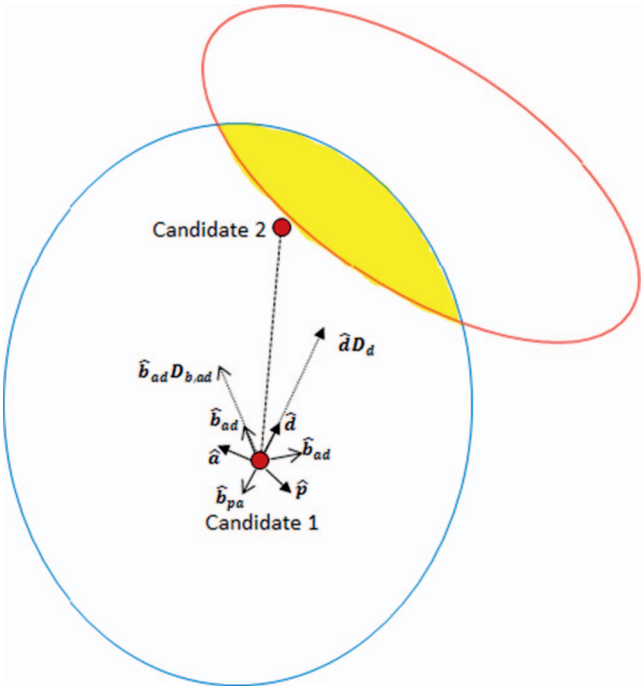

Fig. 3. Graphical representation of Smith chart step vectors used for determination, using (5), of new candidate point when originating candidate possesses acceptable ACPR (blue boundary contour) but unacceptable P_d (red boundary contour).

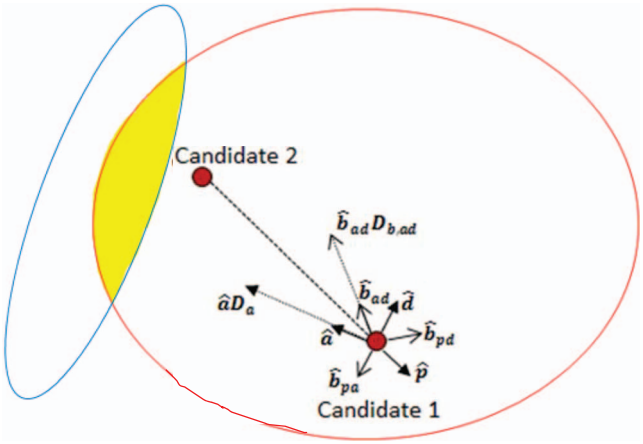

Fig. 4. Graphical representation of Smith chart step vectors used for determination, using (7), of new candidate point when originating candidate possesses acceptable P_d (red boundary contour) but unacceptable ACPR (blue boundary contour).

remaining to this Pareto front. This scenario is illustrated in Fig. 3.

If the present candidate possesses acceptable P_d but unacceptable ACPR, then the search vector becomes

$$\bar{v}- = \hat{a}D_a + \hat{b}_{ad}D_{b,ad}, \tag{7}$$

where D_a is specified by (3) and $D_{b,ad}$ is specified by (6). The component $\hat{a}D_a$ forces the search to improve the value of ACPR, and the component $\hat{b}_{ad}D_{b,ad}$ forces the search toward the Pareto front for ACPR and P_d. This scenario is illustrated in Fig. 4.

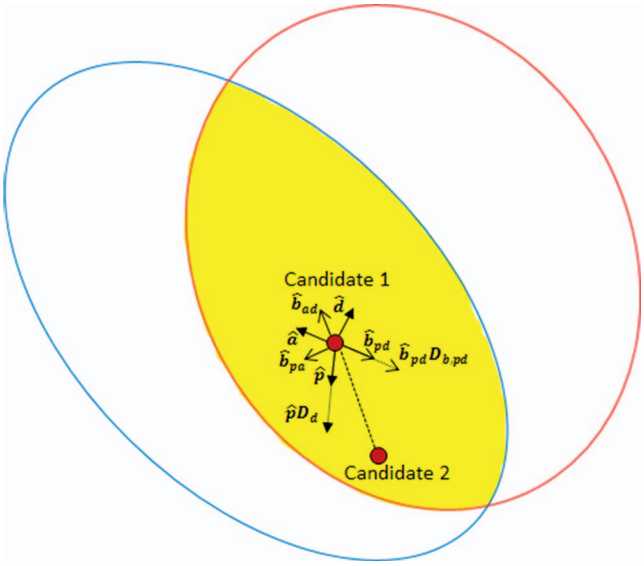

Fig. 5. Graphical representation of Smith chart step vectors used for determination, using (8), of new candidate point when originating candidate possesses acceptable ACPR (blue boundary contour) and P_d (red boundary contour) and $\theta_{pa} < \theta_{pd}$.

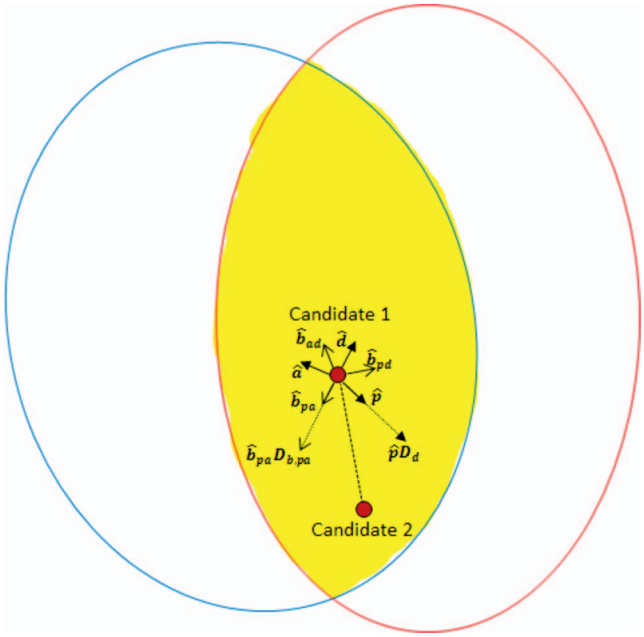

Fig. 6. Graphical representation of Smith chart step vectors used for determination, using (10), of new candidate point when originating candidate possesses acceptable ACPR and P_d and $\theta_{pd} < \theta_{pa}$.

In the previous scenarios described, the objective is to direct the search toward the mutually acceptable region for P_d and ACPR. If the candidate point is already in the mutually acceptable region, two possible situations exist. If θ_{pa}, the smallest angle between $\hat{p}$ and $\hat{a}$, is smaller than θ_{pd}, the smallest angle between $\hat{p}$ and $\hat{d}$, then it can be concluded that the candidate is closer to the Pareto front between P_d and PAE than the Pareto front between ACPR and PAE (Fig. 5). This indicates that the sought constrained optimum is likely on the boundary of P_d

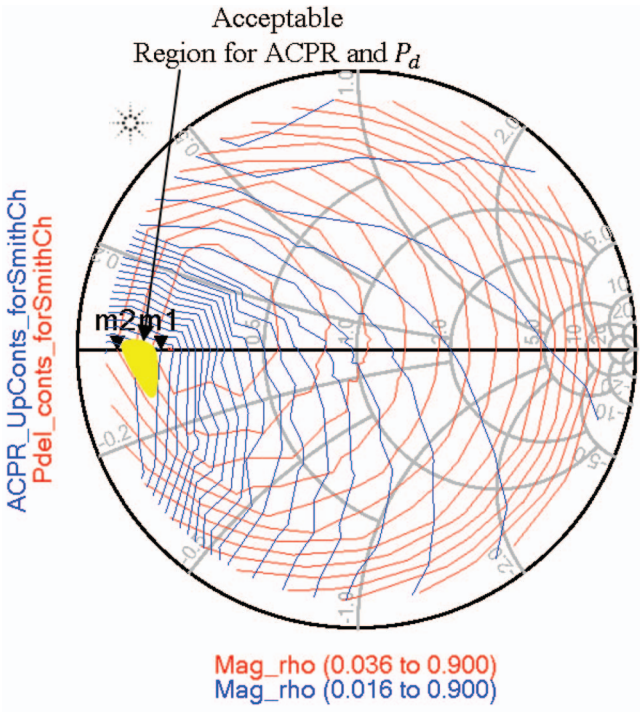

(a)

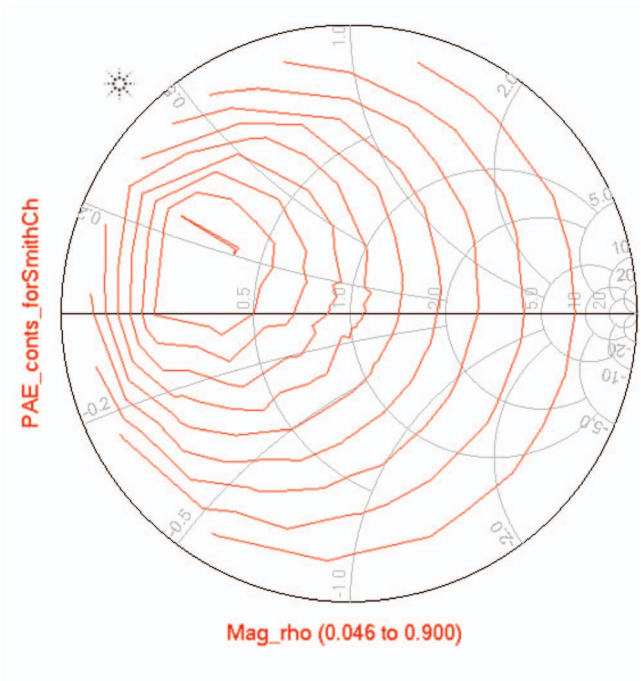

(b)

Fig. 7. Traditionally simulated load-pull contours for (a) ACPR (blue) and P_d (red) and (b) PAE. CDMA 2000 signal is used as excitation. Region of acceptable ACPR and P_d is highlighted.

acceptability. In this case, the search vector to the next candidate is given by

$$\bar{v}- = \hat{p}D_d + \hat{b}_{pd}D_{b,pd} \tag{8}$$

where

$$D_{b,pd} = \frac{D_s}{2}\frac{\left|\theta_{pd} - 90^\circ\right|}{90^\circ}. \quad (9)$$

If instead θ_{pa} is greater than θ_{pd}, then it can be concluded that the candidate is closer to the Pareto front between ACPR and PAE than the Pareto front between P_d and PAE (Fig. 6). In this case, the sought constrained optimum is likely on the boundary of ACPR acceptability. The search vector to the next candidate is given by

$$\bar{v}- = \hat{p}D_a + \hat{b}_{pa}D_{b,pa}, \quad (10)$$

where

$$D_{b,pa} = \frac{D_s}{2}\frac{\left|\theta_{pa} - 90^\circ\right|}{90^\circ}. \quad (11)$$

Using either (8) or (10), the algorithm should converge to the Γ_L providing maximum PAE within the combined acceptable region. If the Pareto front between PAE and one of the other two functions passes through the combined acceptable region, then (8) and (10) will become identical to the equations for the search vector used in our previous PAE/ACPR optimization [14].

Penalties are used to keep the search within the joint acceptable region for ACPR and P_d.

1) If the search begins in one acceptable region, using (5) or (7), and the next candidate does not remain within this same acceptable region, return to the candidate from which this step was taken, divide the search distance parameter D_s by 2, and recalculate to find the next candidate.

2) If in the combined acceptable region, using (8) or (10), and the next candidate is found to be outside the combined acceptable region, return to the candidate from which this step was taken, divide D_s by 2, and recalculate to find the next candidate.

3) If in the combined acceptable region, using (8) or (10), and the next candidate is found to have a lower PAE value, return to the candidate from which this step was taken, divide D_s by 2, and recalculate to find the next candidate.

The search is continued until $|\bar{v}-| < D_n$, the neighboring-point resolution distance, and a Γ_L providing ACPR and P_d within limitations has been found. The largest measured PAE over all measured points that is located in the combined acceptable region is then chosen as the constrained optimum.

III. SIMULATION RESULTS

The algorithm was tested in simulations using Advanced Design System from Keysight Technologies. A nonlinear field-effect transistor model was simulated using the sequential algorithm defined, with a CDMA 2000 broadband input waveform. The main channel is defined with a bandwidth of 1.2288 MHz for this simulation. The adjacent channels are offset by 740 kHz from the center frequency and have 30 kHz bandwidth. The goal of the search was to obtain the Γ_L providing maximum PAE while providing $P_d \geq 32$ dBm and ACPR $\leq$ –46 dBc. For reference, Fig. 7 shows the traditionally simulated load-pull contours for the device. Fig. 7a shows the ACPR and P_d contours, and Fig. 7b shows the PAE contours. As is the case for many devices, the P_d and PAE contours are similar. The boundary region outlined by the limits of ACPR and P_d acceptability is highlighted in Fig. 7a.

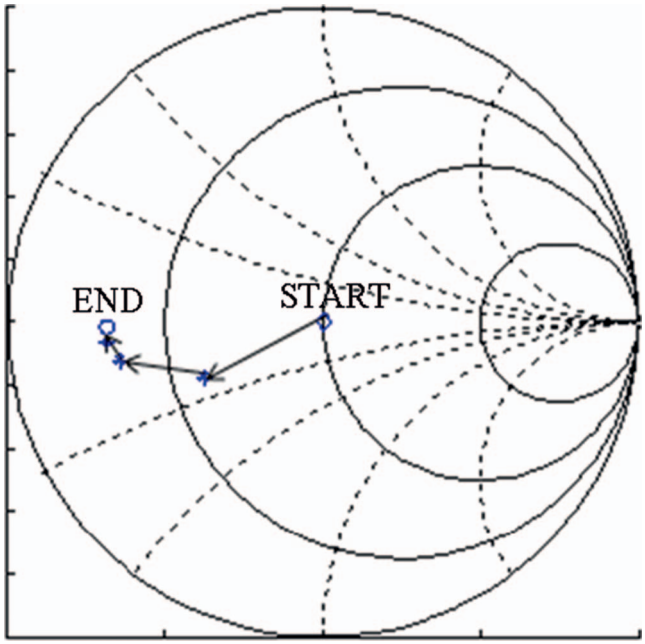

Fig. 8. Simulation search trajectory for starting $\Gamma_L = 0$. Search converges to constrained optimum at $\Gamma_L = 0.69/\underline{-179^\circ}$, requiring total of 13 measurements. Constrained optimum PAE is 34.60%, with final ACPR = –46.17 dBc and $P_d = 34.60$ dBm.

Fig. 8 shows the results of the simulation search for starting reflection coefficient $\Gamma_L = 0$. A total of 13 measurements was required to obtain the constrained optimum. The constrained optimum possesses ACPR and P_d values within the specified constraints, as desired. Figs. 9–12 show the results obtained from different starting points around the Smith chart. Table I provides comparison of the results obtained from the different search starting points.

Table I shows that the optimization results are similar in their end values of Γ_L, ACPR, P_d, and PAE. In these measurements, it is expected that either ACPR or P_d will be limited by its constraint value at the end of the search. For this device and these settings, the ACPR limit is the constraint that is encountered by the search (ACPR is constrained to be less than or equal to –46 dBc). The variation in PAE values is only slight, and such variation is possible in the slight variations of Γ_L endpoint seen in Table I. The number of measurements varies from nine to 25 for the five starting points used in this experiment. The value of P_d is significantly above the constraint of 32 dBm in all cases, which supports the expectation that ACPR is the limiting parameter in this case.

TABLE I
Simulation Results for Different Starting Reflection Coefficients

Start Γ_L	Start ACPR (dBc)	Start P_d (dBm)	Start PAE (%)	End Γ_L	End ACPR (dBc)	End P_d (dBm)	End PAE (%)	No. Measurements
0	–38.35	32.01	24.08	0.69/–179°	–46.17	34.60	33.41	13
0.9/0°	–36.81	19.99	0.08	0.70/–178°	–46.31	34.53	32.74	25
0.9/90°	–36.00	23.24	3.72	0.68/–175°	–46.22	34.41	31.88	22
0.9/180°	–46.96	31.05	13.52	0.73/178°	–46.50	34.56	32.67	9
0.9/–90°	–38.28	22.46	0.78	0.71/179°	–46.17	34.66	33.76	25

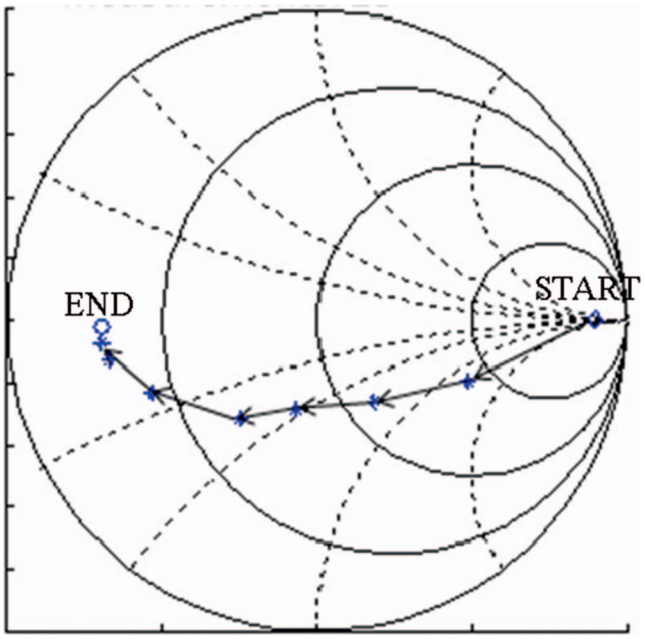

Fig. 9. Simulation search trajectory for starting $\Gamma_L = 0.9/0°$. Search converges to constrained optimum at $\Gamma_L = 0.70/–178°$, requiring total of 25 measurements. Constrained optimum PAE is 32.74%, with final ACPR = –46.31 dBc and $P_d = 34.53$ dBm.

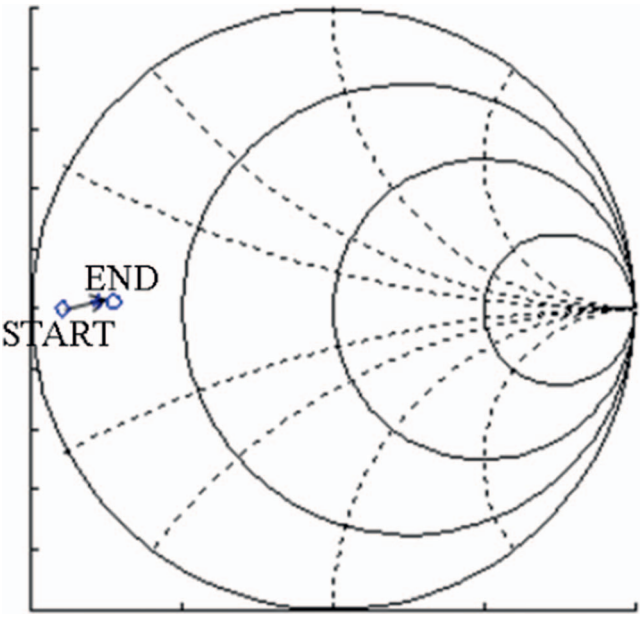

Fig. 11. Simulation search trajectory for starting $\Gamma_L = 0.9/180°$. Search converges to constrained optimum at $\Gamma_L = 0.73/178°$, requiring total of nine measurements. Constrained optimum PAE is 32.67%, with final ACPR = –46.50 dBc and $P_d = 34.56$ dBm.

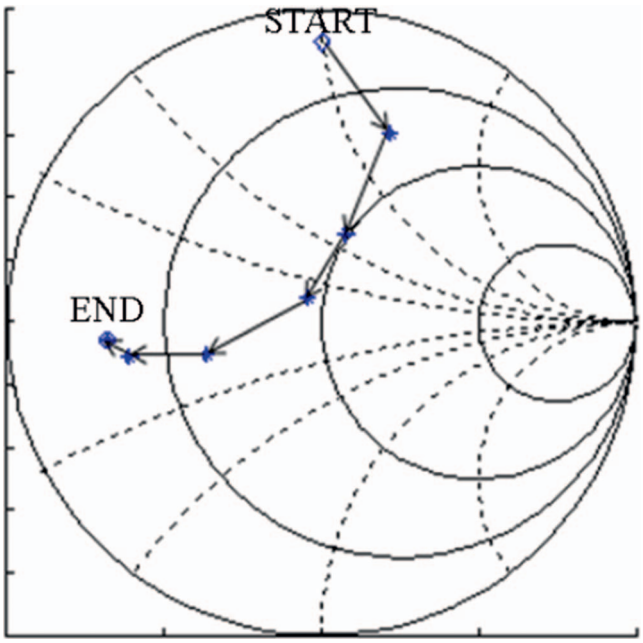

Fig. 10. Simulation search trajectory for starting $\Gamma_L = 0.9/90°$. Search converges to constrained optimum at $\Gamma_L = 0.68/–175°$, requiring total of 22 measurements. Constrained optimum PAE is 31.88%, with final ACPR = –46.22 dBc and $P_d = 34.41$ dBm.

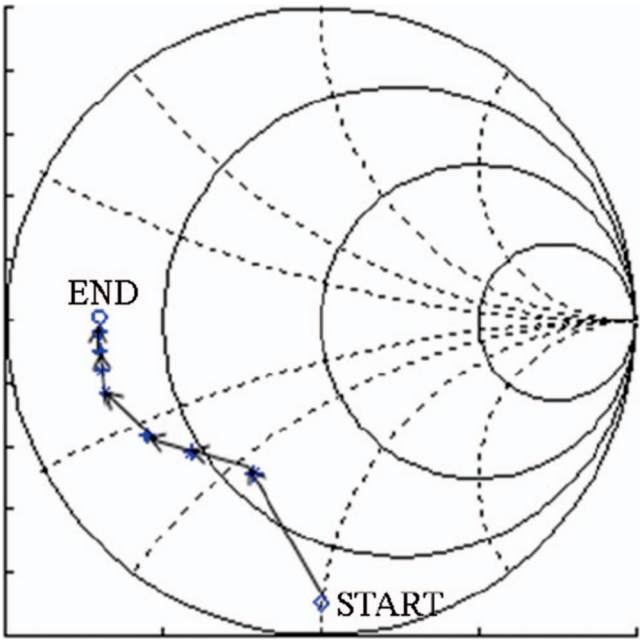

Fig. 12. Simulation search trajectory for starting $\Gamma_L = 0.9/–90°$. Search converges to constrained optimum at $\Gamma_L = 0.707/179°$, requiring total of 25 measurements. Constrained optimum PAE is 33.76%, with final ACPR = –46.17 dBc and $P_d = 34.66$ dBm.

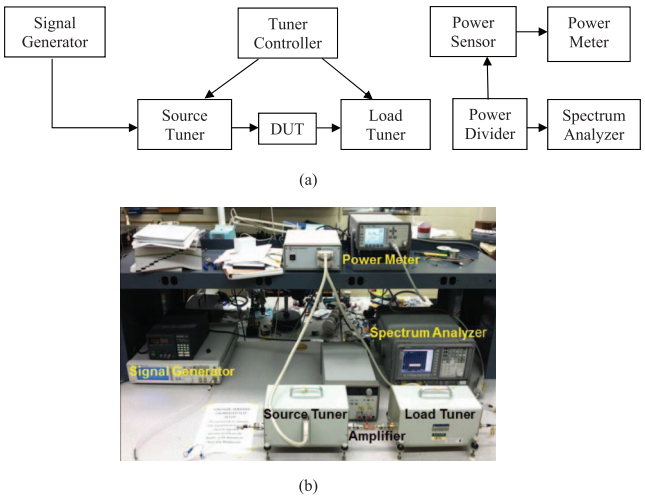

Fig. 13. Measurement setup: (a) block diagram and (b) photo.

IV. MEASUREMENT RESULTS

The algorithm was tested in measurement using a Skyworks 65017-70LF InGaP packaged amplifier. The algorithm was coded in MATLAB, which is used to control load-pull measurements using an automated tuner system from Maury Microwave, in conjunction with Keysight Technologies power sensor and spectrum analyzer. The laboratory measurement bench is shown in Fig. 13. PAE is measured using the power sensor and power meter, in conjunction with the automated bias supply. ACPR is measured by the spectrum analyzer. The spectrum analyzer is placed in ACPR mode, with the main and adjacent channels given a fixed definition for all measurements during the course of the algorithm.

For the measurement optimization, the goal of the search was to obtain the Γ_L providing maximum PAE while providing $P_d \geq 17$ dBm and ACPR $\leq$ –27.5 dBc. The optimization algorithm was tested from multiple starting Γ_L values, with a modified chirp of bandwidth 16 MHz used as the input signal. The main and adjacent channels were each defined to have 10 MHz bandwidth, and the adjacent channel for measurements is offset by 20 MHz from the center frequency. To provide a standard for examining the optimization results, Fig. 14 shows traditionally measured load-pull contours for the Skyworks amplifier. The region of the Smith chart providing acceptable values of ACPR and P_d is shaded. This area is the intersection of the regions providing the required P_d and ACPR values.

Fig. 15 shows the measurement results of the search for a starting reflection coefficient $\Gamma_L = 0$. From this starting point, the search converges with a total of 17 measurements. Figs. 16–19 show the measured search trajectories from additional starting points on the Smith chart. The results obtained from measurement testing of the algorithm from multiple starting points are summarized in Table II. For each starting point, the ACPR is the limiting constraint, and the ACPR values of the

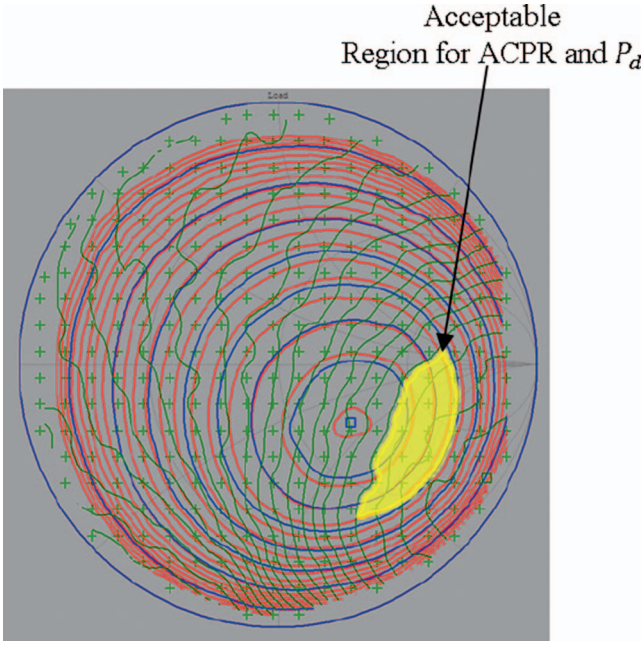

Fig. 14. Traditionally measured load-pull contours for PAE, ACPR, and P_d. Region providing $P_d \geq 17$ dBm and ACPR $\leq$ –27.5 dBc is shaded. This is region bounded by $P_d = 17$ dBm and ACPR = –27.5 dBc contours. PAE contours are displayed in blue, ACPR contours are displayed in green, and P_d contours are displayed in red.

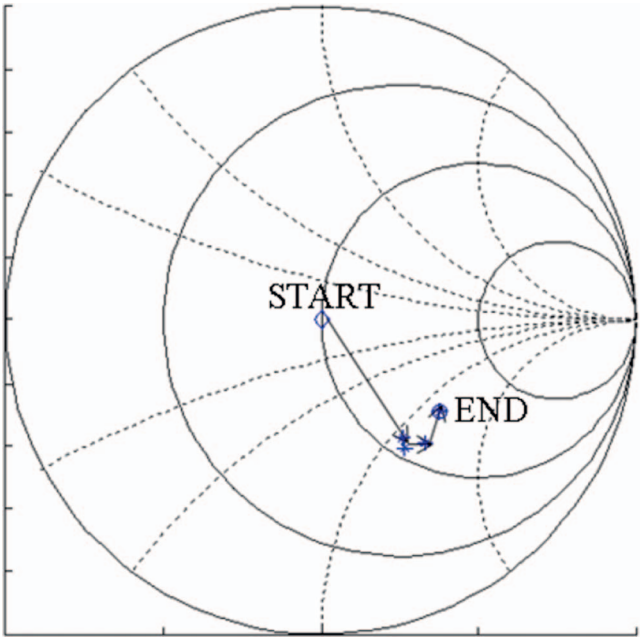

Fig. 15. Measurement search trajectory for starting $\Gamma_L = 0$. Search converges to constrained optimum at 0.47/–37°, requiring total of 17 measurements. Constrained optimum PAE is 7.78%, with final ACPR = –27.77 dBc and $P_d = 18.54$ dBm.

endpoints are all very close to the constraint value of –27.5 dBc. The final values of PAE all correspond (within tenths of a percentage point), and the optima selected by the search are all in close proximity on the Smith chart.

In cases such as these where the PAE and P_d contours are of similar shape, and the maxima for these objective

TABLE II
Measurement Results for Different Starting Reflection Coefficients

Start Γ_L	Start CPR (dBc)	Start P_d (dBm)	Start PAE (%)	End Γ_L	End ACPR (dBc)	End P_d (dBm)	End PAE (%)	No. Measurements
0	–24.33	17.90	6.70	0.47/–37°	–27.77	18.54	7.78	17
0.9/0°	–28.69	10.31	1.02	0.46/–33°	–27.51	18.62	7.92	11
0.9/90°	–22.66	8.25	0.57	0.47/–29°	–27.58	18.57	7.82	28
0.9/180°	–20.63	9.25	0.75	0.52/–33°	–27.85	18.44	7.59	19
0.9/–90°	–23.23	11.79	1.44	0.51/–51°	–27.56	18.38	7.46	10

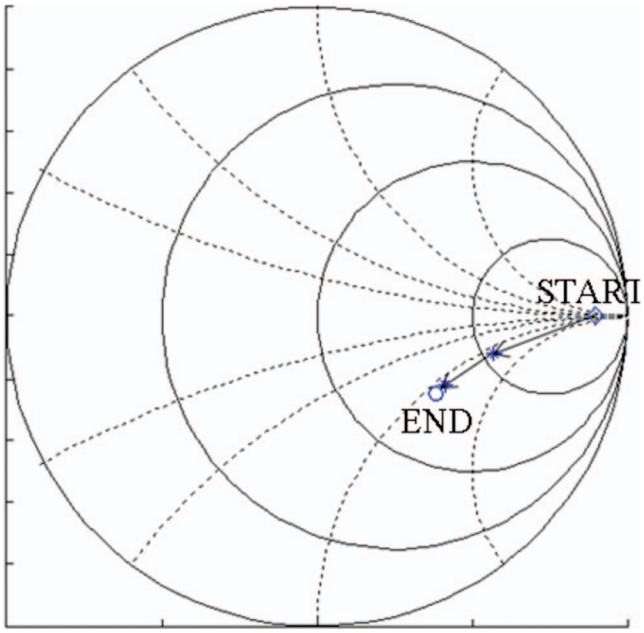

Fig. 16. Measurement search trajectory for starting $\Gamma_L = 0.9/0°$. Search converges to constrained optimum at $\Gamma_L = 0.46/–33°$, requiring total of 11 measurements. Constrained optimum PAE is 7.92%, with final ACPR = –27.51 dBc and P_d = 18.62 dBm.

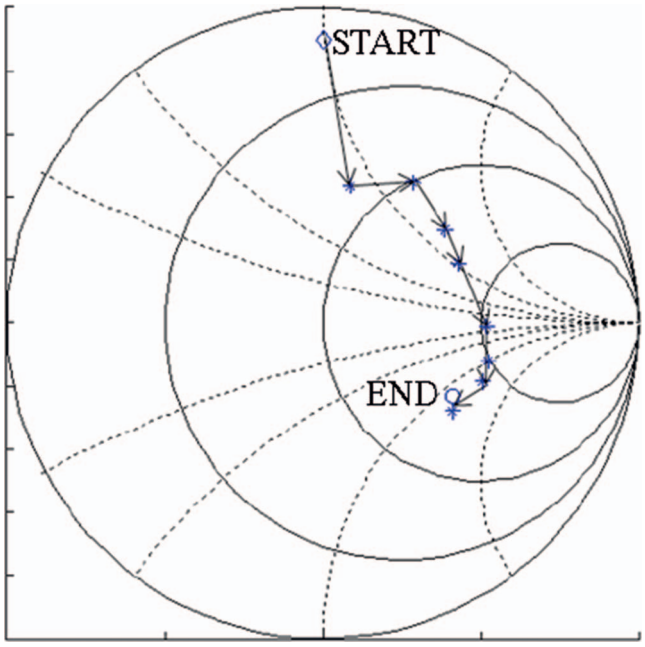

Fig. 17. Measurement search trajectory for starting $\Gamma_L = 0.9/90°$. Search converges to constrained optimum at $\Gamma_L = 0.47/–29°$, requiring total of 28 measurements. Constrained optimum PAE is 7.82%, with final ACPR = –27.58 dBc and P_d = 18.57 dBm.

functions are in close proximity on the Smith chart, it is expected that the constrained optimum will indeed be against the ACPR optimum. However, in certain situations for reduced conduction angle amplifiers where self-biasing is involved (such as Classes B or C), or optimizations involving additional input parameter variations, such as input power or bias voltage, it will be necessary to enforce the output power constraint. For example, the input power could often be reduced to improve PAE in a system, but the P_d criterion must be examined to ensure sufficient power is delivered to meet system specifications. This dual-constraint approach provides a useful framework for such optimizations.

V. CONCLUSIONS

A fast load-pull algorithm has been presented to search for the load reflection coefficient providing maximum PAE while meeting requirements on the ACPR and delivered power. In many radar applications, compliance with spectral constraints (related to the ACPR) and minimum transmitted power requirements (to allow sufficient illumination of the target for detection) must be observed. It is desired to operate the transmitter at the largest efficiency possible while meeting these constraints. Results from simulation and measurement-based searches, taken from multiple starting points, show excellent convergence with between 10 and 28 measured points. The results converge successfully to the region of acceptable ACPR and delivered power in all cases. The search end values of load reflection coefficient and PAE correspond well for different starting points in the simulation and measurement data presented.

This algorithm is expected to find significant application in the real-time optimization of radar transmitter power amplifiers. To do this, onboard sensing and measurement capabilities will be necessary to measure the PAE, ACPR, and delivered power. This paper provides some basic algorithms that could be used in such a system to provide quick adaptation of its power amplifier based on measurements and, potentially, dynamically varying power and spectrum requirements.

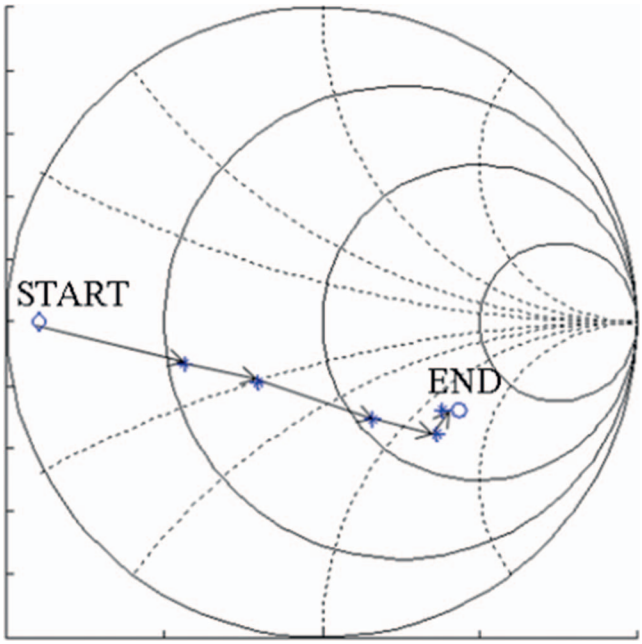

Fig. 18. Measurement search trajectory for starting $\Gamma_L = 0.9/\underline{180^\circ}$. Search converges to constrained optimum at $\Gamma_L = 0.52/\underline{-33^\circ}$, requiring total of 19 measurements. Constrained optimum PAE is 7.59%, with final ACPR = –27.85 dBc and P_d = 18.44 dBm.

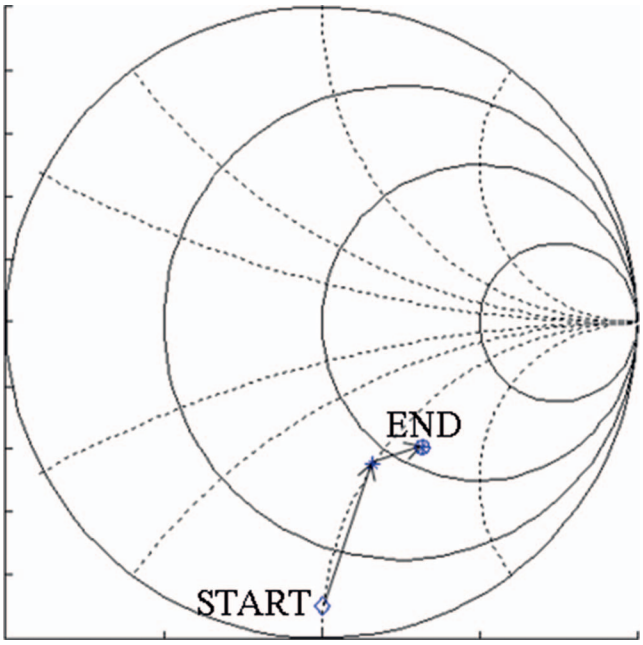

Fig. 19. Measurement search trajectory for starting $0.9/\underline{-90^\circ}$. Search converges to constrained optimum at $\Gamma_L = 0.51/\underline{-51^\circ}$, requiring total of 10 measurements. Constrained optimum PAE is 7.46%, with final ACPR = –27.56 dBc and P_d = 18.38 dBm.

REFERENCES

[1] Brennan, L. E., Reed, I. S.
Theory of adaptive radar.
IEEE Transactions on Aerospace and Electronic Systems, **AES-9**, 2 (Mar. 1973), 237–252.

[2] Blunt, S. D., Cook, M., Jakabosky, J., de Graaf, J. and Perrins, E.
Polyphase-coded FM (PCFM) radar waveforms, Part 1: Implementation.
IEEE Transactions on Aerospace and Electronic Systems, **50**, 3 (Jul. 2014), 2218–2229.

[3] Blunt, S. D., Jakabosky, J., Cook, M., Stiles, J., Seguin, S., and Mokole, E. L.
Polyphase-coded (PCFM) radar waveforms, Part II: Optimization.
IEEE Transactions on Aerospace and Electronic Systems, **50**, 3 (Jul. 2014), 2230–2241.

[4] Kingsley, N., and Guerci, J. R.
Adaptive amplifier module technique to support cognitive RF architectures.
In *Proceedings of the 2014 IEEE Radar Conference*, Cincinnati, OH, May 2014, 1329–1332.

[5] Fu, J.-S., and Mortazawi, A.
Improving power amplifier efficiency and linearity using a dynamically controlled tunable matching network.
IEEE Transactions on Microwave Theory and Techniques, **56**, 12 (Dec. 2008), 3239–3244.

[6] Calpine, H. C., and Golding, A.
Some properties of Pareto-optimal choices in decision problems.
Omega, **4**, 2 (1976), 141–147.

[7] Getachew, T., Kostreva, M., and Lancaster, L.
A generalization of dynamic programming for Pareto optimization in dynamic networks.
RAIRO-Operations Research, **34**, 1 (2000), 27–47.

[8] Marler, R.. T., and Arora, J. S.
Survey of multi-objective optimization methods for engineering.
Structural and Multidisciplinary Optimization, **26**, 6 (2004), 369–395.

[9] Deb, K.
Multi-objective optimization.
In *Search Methodologies*, E. K. Burke and G. Kendall, Eds. New York, NY: Springer, 2005, 273–316.

[10] Das, I., and Dennis, J. E.
Normal-boundary intersection: A new method for generating the Pareto surface in nonlinear multicriteria optimization problems.
SIAM Journal on Optimization, **8**, 3 (Mar. 1998), 631–657.

[11] Kim, I. Y., and de Weck, O.
Adaptive weighted sum method for multiobjective optimization: A new method for Pareto front generation.
Structural and Multidisciplinary Optimization, **31**, 2 (2006), 105–116.

[12] Sevic, J., Burger, K., and Steer, M.
A novel envelope-termination load-pull method for ACPR optimization of RF/microwave power amplifiers.
In *1998 IEEE MTT-S International Microwave Symposium Digest*, **2** (Jun. 1998), 723–726.

[13] Martin, J., Baylis, C., Cohen, L., de Graaf, J., and Marks II, R. J.
A peak-search algorithm for load-pull optimization of power-added efficiency and adjacent-channel power ratio.
IEEE Transactions on Microwave Theory and Techniques, **62**, 8 (Aug. 2014), 1772–1783.

[14] Fellows, M., Baylis, C., Martin, J., Cohen, L., and Marks II, R. J.
Direct algorithm for the Pareto load-pull optimisation of power-added efficiency and adjacent-channel power ratio.
IET Radar, Sonar & Navigation, **8**, 9 (Dec. 2014), 1280–1287.

[15] Iwamoto, M., Williams, A., Chan, P.-F., Metzger, A. G., Larson, L. E., and Asbeck, P. M.
An extended Doherty amplifier with high efficiency over a wide power range.
IEEE Transactions on Microwave Theory and Techniques, **49**, 12 (Dec. 2001), 2472–2479.

[16] Zhang, X., Saycocie, C., Munro, S., and Henderson, G.

A SiGe HBT power amplifier with 40% PAE for PCS CDMA applications.
In *2000 IEEE Microwave Theory and Techniques Society International Microwave Symposium Digest*, **2** (Jun. 2000), 857–860.

[17] Noh, Y. S., and Park, C. S.
PCS/W-CDMA dual-band MMIC power amplifier with a newly proposed linearizing bias circuit.
IEEE Journal of Solid-State Circuits, **37**, 9 (Sep. 2002), 1096–1099.

[18] Kusunoki, S., Yamamoto, K., Hatsugai, T., Nagaoka, H., Tagami, K., Tominaga, N., Osawa, K., Tanabe, K., Sahurai, S., and Iida, T.
Power-amplifier module with digital adaptive predistortion for cellular phones.
IEEE Transactions on Microwave Theory and Techniques, **50**, 12 (Dec. 2002), 2979–2986.

[19] Sevic, J.
Large signal automated load-pull characterization of adjacent-channel power ratio for digital wireless communication systems.
In *1996 IEEE MTT-S International Microwave Symposium Digest*, **2** (Jun. 1996), 763–766.

[20] Wu, Q., Xiao, H., and Li, F.
Linear power amplifier design for CDMA signals: A spectrum analysis approach.
Microwave Journal, 1998, 22–40.

[21] Reveyrand, T., Gasseling, T., Barataud, D., Mons, S., and Nebus, J.-M.
A smart load-pull method to safely reach optimal matching impedances of power transistors.
In *2007 IEEE MTT-S International Microwave Symposium Digest*, Jun. 2007, 1489–1492.

[22] Sun, Y.
Evolutionary tuning method for automatic impedance matching in communication systems.
In *Proceedings of the 1998 IEEE International Conference on Electronics, Circuits, and Systems*, **3** (1998), 73–77.

[23] Sun, Y., and Lau, W. K.
Antenna impedance matching using genetic algorithms.
In *Proceedings of the IEE Conference on Antennas and Propagation*, York, United Kingdom, Aug. 1999, 31–36.

[24] Qiao, D., Molfino, R., Lardizabal, S., Pillans, B., Asbeck, P., and Jerinic, G.
An intelligently controlled RF power amplifier with a reconfigurable MEMS-varactor tuner.
IEEE Transactions on Microwave Theory and Techniques, **53**, 3 (Mar. 2005), 1089–1095.

[25] du Plessis, W., and Abrie, P.
Lumped impedance matching using a hybrid genetic algorithm.
Microwave and Optical Technology Letters, **37**, 3 (May 2003), 201–212.

Matthew Fellows completed the B.S. and M.S. degrees in electrical and computer engineering at Baylor University in 2012 and 2014, respectively. He is currently pursuing his Ph.D. degree at Baylor University. His research is focusing on the creation of algorithms for the joint optimization of radar transmitter power amplifier circuitry and waveforms. He has published several papers related to his areas of interest.

Lucilia Lamers received the B.S. degree in electrical and computer engineering from Baylor University in 2016. She is presently working toward the M.S. degree in electrical engineering at Baylor University. Her research is focused on optimization of tunable matching networks for radar transmitters.

Charles Baylis (S'03 – M'08 – SM'16) is an associate professor of electrical and computer engineering at Baylor University where he directs the Wireless and Microwave Circuits and Systems (WMCS) Program. Dr. Baylis received the B.S., M.S., and Ph.D. degrees in electrical engineering from the University of South Florida in 2002, 2004, and 2007, respectively. His research focuses on spectrum issues in radar and communication systems and has been sponsored by the National Science Foundation, the Army Research Laboratory, and the Naval Research Laboratory. He has focused his work on the application of microwave circuit technology and measurements, combined with intelligent optimization algorithms, to creating reconfigurable transmitters. He founded the annual Texas Symposium on Wireless and Microwave Circuits and Systems and serves as chair of the executive committee for this conference.

Lawrence Cohen (M'87 - SM'12) has been involved in electromagnetic compatibility (EMC) engineering and management, shipboard antenna integration, and radar system design for 33 years. In this capacity, he has worked in the areas of shipboard electromagnetic interference problem identification, quantification and resolution, mode-stirred chamber research, and radar absorption material design, test and integration. In March of 2007 Mr. Cohen acted as the Navy's principal investigator in the assessment of radar emissions on a WiMAX network. Additionally, he has acted as the principal investigator for various radar programs, including the radar transmitter upgrades. Currently, he is involved with identifying and solving spectrum conflicts between radar and wireless systems as well as research into spectrally cleaner power amplifier designs, tube, and solid state.

Mr. Cohen received a B.S. degree in electrical engineering from The George Washington University in 1975 and a M.S. degree in electrical engineering from Virginia Tech in 1994. He is certified as an EMC engineer by the National Association of Radio and Telecommunications Engineers (NARTE). Larry served as the technical program chairman for the IEEE 2000 International Symposium on EMC and was elected for a three-year term to the IEEE EMC Society Board of Directors in 1999 and 2009. He is also a member of the IEEE EMC Society Technical Committee 6 (TC-6) for Spectrum Management. For the past 26 years, he has been employed by the Naval Research Laboratory in Washington, DC. In his spare time he enjoys golf, hiking, cycling, and target shooting.

Robert J. Marks, II (S'71–M'72–SM'83–F'94) is a Distinguished Professor of electrical and computer engineering at Baylor University, Waco, TX, USA. When at the University of Washington, he served for 17 years as the faculty advisor to the student chapter of Campus Crusade for Christ. He is a Fellow of IEEE and the Optical Society of America. His most recent books are Handbook of Fourier Analysis and Its Applications (Oxford University Press, 2009), and Biological Information—New Perspectives (Singapore: World Scientific, 2013), coedited by M. J. Behe, W. A. Dembski, B. L. Gordon, and J. C. Sanford. He has an Erdős-Bacon number of five.